Supporting Information

Eierhoff et al. 10.1073/pnas.1402637111

SI Materials and Methods

Lectin A Incubation and Inhibition and Depletion of Glycosphingolipids. Depletion of plasma membrane (PM)-localized globotriaosylceramide (Gb3) was achieved by 30-min preincubation of cells at 37 °C with 5 $\mu g \cdot mL^{-1}$ Cy3-labeled Shiga toxin B-subunit (StxB). For glycosphingolipid (GSL) depletion, cells were passaged for 3 d in the presence of 5 μM D-threo-l-phenyl-2-palmitoylarmino-3-morpholino-l-propanol (PPMP; Santa Cruz), a substrate analog of the glucosylceramide synthase (1). For lectin LecA inhibition, purified, Alexa488-conjugated LecA (2 $\mu g \cdot mL^{-1}$) or bacteria were preincubated for 15 min at 37 °C with *para*-nitrophenyl-α-D-galactopyranoside (PNPG) (Sigma-Aldrich) at 10 mM final concentration and then incubated with cells for fluorescence microscopic analysis or invasion and adhesion assay, respectively. For confirmation of Gb3 depletion and LecA inhibition, cells were grown on coverslips incubated as described above with Cy3-labeled StxB and PNPG, respectively. Afterward, cells were washed twice with Dulbecco's phosphate-buffered saline (DPBS), incubated with 2 $\mu g \cdot mL^{-1}$ StxB-Alexa488 or LecA-Alexa488 for 30 min at 37 °C. After incubation all cells were washed, fixed with 4% paraformaldehyde and stained for actin by Phalloidin-ATTO647N (Sigma-Aldrich).

Generation of Stable Cell Lines. The human lung epithelial cell line H1299 (American Type Culture Collection no. CRL-5803) was grown in RPMI medium, supplemented with 10% FCS and L-glutamine at 37 °C and 5% CO_2. For cultivation of MDCKII cells we used DMEM supplemented with 5% FCS and L-glutamine. For the generation of stable cell lines H1299 cells were transfected with a GPI-mCherry or LifeAct-mCherry encoding plasmid and MDCKII cells were transfected with a Gb3-synthase encoding plasmid. Both plasmids additionally encode for a Geneticin resistance. For stable expression of GPI-mCherry and Gb3-synthase, positive clones were selected and continuously cultivated in RPMI or DMEM supplemented with 500 $\mu g \cdot mL^{-1}$ Geneticin, L-glutamine, and 10% FCS (for H1299 cells) or 5% FCS (for MDCKII cells). For the detection of Gb3, MDCKII cells were trypsinized, washed once with DPBS, incubated for 30 min at 37 °C with StxB-Alexa488 (12 $\mu g \cdot mL^{-1}$), washed again twice with DPBS, and subjected to FACS.

GFP Tagging and Deletion of *lecA* in *Pseudomonas aeruginosa*. GFP-tagged *P. aeruginosa* PAO1 WT and PAO1 Δ*lecA* were constructed as followed: PCR was used to generate a 479-bp DNA fragment upstream of the *lecA* gene, with the (DellecAUp5A-CCCCGTGCCGGTTCGACCCCGGC, DellecAUp3GGTTGG-CAGGCCACCCCGTG) oligonucleotide pairs and a 468-bp DNA fragment downstream of the *lecA* using the (DellecADn5-CAAGTTATCACCAAGCATGATTGATCTC, DellecADn3-CATGGCTTGGTGATAACTTGTCTCGGAAAA) oligonucleotide pairs. The resulting DNA fragments were further used as templates for a second overlapping PCR run using a pair of external oligonucleotides (DellecAUp5 and DellecADn3), thus leading to a final approximate 1.1-kb DNA fragment that was cloned into the pCR2.1 vector. The resulting DNA fragment bearing appropriate sites, namely, BamHI/EcoRV, was further hydrolyzed and cloned into the suicide vector pKNG101. The recombinant plasmid was then mobilized into *P. aeruginosa* and the deletion mutant was selected on LB plates containing 6% sucrose and streptomycin. The *P. aeruginosa* strains, the *Escherichia coli* donor strain harboring a plasmid containing miniTn7Δ*gfp* (Gm cassette), and the two *E. coli* helper strains harboring pRK600 and pUX-BF13 were grown overnight at 37 °C in LB, in the presence of the required antibiotics. This protocol is similar to the three-partner mating but with a longer period of incubation at 42 °C for the recipient strain and overnight contact. *P. aeruginosa* stocks were prepared by inoculating LB–Miller medium containing 60 $\mu g \cdot mL^{-1}$ Gentamicin with material of a single colony of *P. aeruginosa* grown on HiFluoro *Pseudomonas* Agar Base (Sigma-Aldrich), incubated overnight at 37 °C, mixed with glycerol (30% vol/vol), aliquoted, and stored at −80 °C. For experiments, LB–Miller medium containing 60 $\mu g \cdot mL^{-1}$ Gentamicin was inoculated with *P. aeruginosa* of a stock aliquot incubated at 37 °C on a Thermomixer (PeqLab) at 650 rpm for 16–20 h to ensure that LecA was efficiently expressed (2). The growth kinetic of *P. aeruginosa* was recorded in a 96-well plate containing LB medium by measurement of the OD at 600 nm in a Tecan Safire Plate Reader (Tecan). LecA expression was tested by standard Western blotting using LecA-specific, polyclonal rabbit antibody.

Invasion and Adhesion Assay. Overnight cultures of bacteria were pelleted and resuspended in RPMI or DMEM for infection of H1299 and MDCKII cells, respectively, containing additionally 1 mM $CaCl_2$ and $MgCl_2$. Bacteria were incubated for 2 h at 37 °C with cells (70–80% confluent) at a multiplicity of infection (MOI) of 100. Cells were washed three times with DPBS. Extracellular bacteria were inactivated by a 2-h treatment of cells at 37 °C with 400 $\mu g \cdot mL^{-1}$ Amikacin sulfate (Sigma-Aldrich). Afterward, cells were washed two times with DPBS and lysed with 0.25% (vol/vol) Triton X-100 at 37 °C. Cell extracts were plated on Gentamicin-containing (60 $\mu g \cdot mL^{-1}$) LB–Miller Agar plates and incubated over night at 37 °C. The next day bacterial colonies were counted. Invasion was calculated as percentage of Amikacin-survived bacteria compared with the total number of bacteria associated with Amikacin-untreated cells. For comparison purposes mean values of $n \geq 3$ independent experiments were normalized to the invasion of untreated, WT bacteria. Invasion and adhesion assays with *lecA*- and non-*lecA*-expressing *E. coli* strains were performed as described above. Instead of Amikacin, 100 $\mu g \cdot mL^{-1}$ Gentamicin was used for 1 h at 37 °C. For adhesion assays cells were inoculated with bacteria at 4 °C for 1 h, afterward washed three times with cold DPBS, lysed, and plated as described for the invasion assay.

Inhibition of Actin Polymerization. Inhibition of actin polymerization was achieved by two complementary approaches: knockdown of actin-related protein 2 (Arp2) and treatment of H1299 cells with latrunculin A (Sigma-Aldrich), a compound that binds to monomeric actin, thereby preventing actin polymerization. Knockdown of Arp2 was achieved by transfecting 5×10^5 H1299 cells two times within 3 d with 200 pmol siRNA (Santa Cruz) using Lipofectamine 2000 (Invitrogen). The knockdown efficiency was tested by Western blot analysis using an Arp2-specific antibody (Santa Cruz). Three days posttransfection, cells were inoculated with *P. aeruginosa* PAO1 WT for fluorescence microscopy analysis or invasion assays as described. Latrunculin A was applied at 0.1 μM final concentration 15 min before and during inoculation with *P. aeruginosa* PAO1 WT.

Plasma Membrane Spheres. For plasma membrane spheres (PMS) studies, we used H1299 cells stably expressing LifeAct-mCherry to visualize actin polymerization (3). PMS buffer contained 10 μM (final concentration) of MG132 (Sigma). Cells were

incubated with PMS buffer for 13–16 h at 37 °C. Subsequently, cells were incubated for 1 min at room temperature with FM4-64 Dye [N-(3-triethylammoniumpropyl)-4-(6-(4-(diethylamino) phenyl) hexatrienyl) pyridinium dibromide; Life Technologies]in PMS buffer (dilution: 1:10,000) to visualize the PM. After replacement by fresh PMS buffer cells were inoculated with bacteria to perform confocal microscopy.

Cholesterol Depletion. Cellular cholesterol was depleted by preincubation of cells at 37 °C with 10 mM methyl-β-cyclodextrin (MCD) for 30 min. Afterward, cells were washed once with DPBS and inoculated with *P. aeruginosa* PAO1 WT to conduct invasion assays or microscopic analyses.

Microscopic Imaging. Cells, GUVs, and *P. aeruginosa* infection were imaged on a confocal microscope (Nikon Eclipse Ti-E with A1R confocal laser scanner, 60× oil objective, N.A. 1.49). Image acquisition and analysis was performed with NIS-Elements (Nikon). For visualization of cellular infection, H1299 GPI-mCherry or H1299 LifeAct-mCherry cells grown on glass coverslips or in CELLview dishes (Greiner) were inoculated for 0.5 and 1 h at 37 °C, respectively, with *P. aeruginosa* with an MOI of 100. Afterward, cells were washed once with DPBS, fixed, and stained for actin by phalloidin-ATTO 647N (Sigma-Aldrich) and Arp2 using an Arp2-specific rabbit antibody (Santa Cruz) detected by an anti-rabbit Alexa405 (Life Technologies) secondary antibody. Live cell imaging was performed at 37 °C by using an incubator stage mounted onto the microscope (Okolab). For visualization of GUVs, images were recorded using the resonant scanning mode of the A1R confocal.

GUV Preparation. GUVs were prepared by the electroformation technique at room temperature on indium-tin oxide (ITO)-coated slides. If not indicated otherwise all lipid preparations contain 30 mol% cholesterol (Avanti Polar Lipids), 0.25 mol% DHPE-TR (Life Technologies), and indicated concentrations of Gb3 (Matreya LLC). Additionally, lipid mixtures contain 1,2-dioleoyl-*sn*-glycero-3-phosphocholine (DOPC) (Avanti Polar Lipids) of the following concentrations: 64.75 mol% for 5 mol% Gb3-mixtures, 68.75 mol% for 1 mol% Gb3, 69.65 mol% for 0.1 mol% Gb3, 69.25 mol% for 0.5 mol% Gb3, 69.74 mol% for 0.01 mol% Gb3, and 69.75 mol% for 0 mol% Gb3. Cholesterol-free GUVs contained 94.75 mol% DOPC, 5 mol% Gb3, and 0.25 mol% DHPE–Texas Red. Lipid mixtures were dissolved in chloroform (0.5 mg·mL^{-1}) and 15 μL was spread on the conductive faces of the ITO slides. After at least 2 h of drying under vacuum, GUVs were grown in a 290 mOsm·L^{-1} sucrose solution by applying an alternating electric field from 20 mV to 1.1 V for 3 h. Surface tension of GUVs was decreased by increasing the osmolarity of the outer GUV buffer, which was adjusted to 550 mOsm·L^{-1}. Bacteria were incubated with GUVs at room temperature and examined on the inverted confocal fluorescence microscope.

Physical Model. The mechanical Helfrich energy associated with an elastic membrane is, per unit area,

$$e=\gamma+2\kappa H^2,\quad H=\frac{1}{2}\left(\cos(\psi)\frac{\mathrm{d}\psi}{\mathrm{d}r}+\frac{\sin(\psi)}{r}\right), \qquad \textbf{[S1]}$$

with surface tension γ, bending rigidity κ, mean curvature H (4), and angle ψ and radius r as defined in Fig. 2*A*. For a surface element $2\pi r(s)\,\mathrm{d}s$ the Helfrich energy and adhesion energy, as opposed to the unbound plane membrane, are with the adhesion energy per Gb3:

$$\begin{aligned}
2\kappa H(s)^2\cdot 2\pi r(s)\mathrm{d}s &= 2\pi\kappa\left(2\left(RH(s)\right)^2\tilde{r}(\tilde{s})\mathrm{d}\tilde{s}\right) && \text{(bending)}\\
\gamma(1-\cos\psi)\cdot 2\pi r(s)\mathrm{d}s &= 2\pi\kappa\left(\tilde{\gamma}(1-\cos\psi)\tilde{r}(\tilde{s})\mathrm{d}\tilde{s}\right) && \text{(surface tension)}\\
-\epsilon\rho\cdot 2\pi r(s)\mathrm{d}s &= 2\pi\kappa\left(-\tilde{\epsilon}\tilde{\rho}\tilde{r}(\tilde{s})\mathrm{d}\tilde{s}\right) && \text{(adhesion energy).}
\end{aligned}$$

Lipid ε, the local Gb3 surface density ρ, the cylinder radius R, and the geometry are as defined in Fig. 2*A*. On the right-hand side we have rescaled the lengths by R, surfaces by $2\pi R^2$ (and surface densities by the inverse), γ by κR^{-2}, and energies by $2\pi\kappa$. The cylinder surface fraction where the membrane and the rod-shaped particle are in contact is $A=2\pi Rh$ and, after rescaling, $\tilde{A}=h/R=\tilde{h}$. We replace $\tilde{A}$ by $\tilde{h}$ and omit the tilde for rescaled quantities in the following. The rescaled free energy is

$$F_m(h)=\int\left(\left(2(RH(s))\right)^2+\gamma\left(1-\cos\psi(s)\right)-\epsilon\rho(h)\right)r(s)\mathrm{d}s, \qquad \textbf{[S2]}$$

where the integral is carried out over the cylinder surface fraction h. The contribution of the free membrane part—the part not attached to the cylinder—cannot be treated analytically. However, the contribution of this part is always very small, as we confirmed by numerical integration (5). To make progress we neglect this part in what follows. In Fig. S4*A* we compare the full free energy with the approximation neglecting the free membrane part. After integration we obtain

$$F_m(h)=\begin{cases}
h\left(2-\epsilon\rho(h)\right)+\frac{1}{2}\gamma h^2 & \text{for } 0\le h\le 1\\
h\left(\frac{1}{2}-\epsilon\rho(h)+\gamma\right)+\frac{3}{2}-\frac{1}{2}\gamma & \text{for } 1\le h\le L+1\\
h\left(2-\epsilon\rho(h)\right)+\frac{1}{2}\gamma(h-L)^2+L\left(\gamma-\frac{3}{2}\right) & \text{for } L+1\le h\le L+2.
\end{cases} \qquad \textbf{[S3]}$$

Considering N Gb3 lipids (M DOPC lipids) on the vesicle with surface V from which n (m) lipids lie within the surface fraction h we can write the relations between areas and lipid numbers

$$V=Na+Mb,\quad h=na+mb \qquad \textbf{[S4]}$$

with the surface areas a and b of Gb3 and DOPC, respectively. The entropy of the noninteracting particles is proportional to the logarithm of the number of characteristic microstates:

$$S(h,\rho)=\ln\left(g(n,m,N,M)\right),\quad g=\binom{n+m}{n}\times\binom{N-n+M-m}{N-n} \qquad \textbf{[S5]}$$

with the local and average Gb3 densities $\rho=n/h$ and $\sigma=N/V$. The entropy loss is

$$F_l(h,\rho)=\frac{k_{\mathrm{B}}T}{2\pi\kappa}\left(S(\rho)-S(\sigma)\right)=:K\left(S(\rho)-S(\sigma)\right). \qquad \textbf{[S6]}$$

Note that it does not matter whether the mixing entropy is derived in the microcanonical ensemble, as we do it here, or in the canonical ensemble. Using the Stirling formula and Eq. **S4** we obtain for the derivative

$$\begin{aligned}
\frac{1}{Kh}\frac{\partial F_l}{\partial\rho}=&\frac{a}{b}\log\left(1+\frac{b\rho}{1-a\rho}\right)-\frac{a}{b}\log\left(1+\frac{b(V\sigma-A\rho)}{V-A-a(V\sigma-A\rho)}\right)\\
&-\log\left(\frac{b-a}{b}+\frac{1}{b\rho}\right)+\log\left(\frac{b-a}{b}+\frac{V-A}{b(V\sigma-A\rho)}\right).
\end{aligned} \qquad \textbf{[S7]}$$

By minimizing $F_l + F_m$ for fixed h we obtain the local density ρ_0. With the simplification $b = a$ we can obtain a closed expression

$$\frac{\partial F_m}{\partial \rho}+\frac{\partial F_l}{\partial \rho}=0 \quad \Rightarrow \quad \rho(\sigma)=\frac{\nu(\sigma)-\sqrt{\nu(\sigma)^2-4Vha\sigma\alpha(\alpha-1)}}{2ha(\alpha-1)} \tag{S8}$$

with $\alpha = \exp(\varepsilon/K)$ and $\nu(\sigma) = V + (\alpha - 1)(Va\sigma + h)$. Further progress with these results turns out to be difficult (i.e., analytical progress would be blocked and one would have to refer to numerical methods). However, the steric repulsion between the particle is only important for high local densities, that is, as long as the local density is low one could treat the lipids as point particles. Of course the local density is unknown a priori because it results from the minimization of the free energy. A possible route out of this dilemma is to approximate the lipids as point particles, calculate h, and check subsequently the validity of the approximation.

In the following we derive the mixing entropy of point-like particles in the canonical ensemble:

$$\mathcal{Z}(T,V,N)=\frac{1}{N!}\left(\frac{V}{l^2}\right)^N, \quad F(T,V,N)=-\frac{k_BT}{2\pi\kappa}\ln\left(\mathcal{Z}(T,V,N)\right), \tag{S9}$$

with some length l. Again, we use the Stirling formula, add the free energies for the surface fractions h and $V - h$, subtract the free energy for $\rho = \sigma$, and obtain

$$F_l(h,\rho)=Kh\rho\ln\left(\frac{\rho}{\sigma}\right)+KV\sigma\left(1-\frac{h\rho}{V\sigma}\right)\ln\left(\frac{1-\frac{h\rho}{V\sigma}}{1-\frac{h}{V}}\right) \tag{S10}$$

$$\Rightarrow \quad \rho=\frac{\sigma\alpha}{1+\frac{h}{V}(\alpha-1)}.$$

Substituting ρ into Eqs. **S3** and **S10** the wrapping height follows from

$$0=F_m'(h)+F_l'(h)$$
$$=\begin{cases} -\frac{K\sigma(\alpha-1)}{1+(\alpha-1)h/V}+2+\gamma h & \text{for} \quad 0\le h\le 1 \\ -\frac{K\sigma(\alpha-1)}{1+(\alpha-1)h/V}+\frac{1}{2}+\gamma & \text{for} \quad 1\le h\le L+1 \\ -\frac{K\sigma(\alpha-1)}{1+(\alpha-1)h/V}+2+\gamma(h-L) & \text{for} \quad L+1\le h\le L+2 \end{cases}. \tag{S11}$$

To verify the validity of this result, we numerically calculated the full free energy (including the numerically evaluated free membrane part in Eq. **S2** and the free energy for the lattice gas in Eq. **S6**) for different surface densities σ. Fig. S4*A* depicts the good agreement between the simplified energies for point particles, the corrected energy for the lattice gas, and the full free energy. For small densities, the contribution of the free membrane part dominates the deviations, whereas the saturating density of the lattice gas (Fig. S4*C*) becomes important for increasing densities. It can be seen that the approximations done only introduce a minor error. Further, we show in Fig. S4*B* the relative error of the local density ρ_P, if one treats the lipids as point particles and ignores the steric repulsion, in comparison with the saturating local densities ρ for the lattice gas. The relative error is in the relevant regime always smaller than 5%, which justifies the point-particle approximation.

Critical GUV Diameters for Full Wrapping. For larger vesicles, entropy loss becomes less important owing to the larger surface reservoir. By solving Eq. **S11** with respect to the diameter of the vesicle, we achieve an expression for the minimal or critical diameter d_c for which the bacteria is at least wrapped up to a height h as a function of the system parameters. For the case of full wrapping ($h = L + 2$) and of wrapping just up to the lower boundary of the spherical cap ($h = L + 1$), one obtains

$$d_c(h=L+1)=R\sqrt{\frac{18(\alpha-1)}{K\sigma(\alpha-1)/(0.5+\gamma)-1}} \tag{S12}$$

$$d_c(h=L+2)=R\sqrt{\frac{20(\alpha-1)}{K\sigma(\alpha-1)/(2+2\gamma)-1}}. \tag{S13}$$

Owing to the dynamics of the GUV system and resultant technical challenges we were unable to clearly resolve the extent of wrapping. In addition, the global Gb3 concentrations on the vesicles might vary owing to lipid heterogeneities during GUV preparation. The resulting uncertainty regime of the critical vesicle diameter is shown in Fig. 2*D*. The lower boundary of the uncertainty regime was calculated by using $d_c(h = L + 1)$ with 40% increased Gb3 concentration and the upper boundary by using $d_c(h = L + 2)$ with 40% decreased Gb3 concentration. The surface tension was fixed to $\gamma = 800$ μJ/m^2 in both cases.

Values. The calculations were carried out at room temperature ($T = 293$ K). The bending rigidity for typical phospholipid bilayers is $\kappa = 20\ k_BT$ (see refs. 6 and 7). The surface tension of the GUVs lies within $\gamma = 10^{-6}$ to 10^{-3} J/m^2 (8). Microcalorimetry titration shows that the free energy gain owing to the binding of Gb3 (αGal1-4βGal1-4Glc) to LecA (PA-IL) is $-\Delta G = 5.6$ kcal/mol (9), which is equivalent to an adhesion energy $\varepsilon \approx 9.6\ k_BT$ per lipid.

In GUV experiments, the bilayer contained 65 mol% DOPC and 5 mol% Gb3. The area per lipid of Gb3 and DOPC in a bilayer is $a = 80$ Å^2 (10) and $b = 67.4$ Å^2 (11), respectively. Thus, the surface concentration of Gb3 was $\sigma \approx 10^5$ μm^{-2} on average and may not surpass 1.25 nm^{-2}.

The fraction of glycosphingolipids in the plasma membrane is believed to be ~1–5% of all lipids. For Gb3, 0.1–0.5% seems plausible, so we expect the average surface density of Gb3 within the range $\sigma = 1{,}400$–$7{,}400$ μm^{-2}.

Clustering of Gb3 Lipids. During the wrapping process of the bacteria Gb3 lipids are recruited to the wrapping region and thereby enhance the adhesion energy and subsequently the wrapping height. The local density of Gb3 lipids is shown in Fig. S4*C* as a function of the global Gb3 density σ and the diameter of the GUV. Owing to the recruiting mechanism bacteria are fully wrapped at a lower global Gb3 density compared with the case of immobile lipids (Fig. 2*C*). This effect is more pronounced for larger vesicles, because the Gb3 lipid reservoir is larger compared with smaller vesicles. Although the clustering of Gb3 lipids is important for the wrapping process, the local density does not saturate before the bacteria are fully wrapped. This can be seen by comparing Fig. 2*C* and Fig. S4*C*. For example, a global Gb3 density of $\sigma = 0.001$ nm^{-2} results for a GUV of 50-μm diameter (red curve) in a fully wrapped bacteria, whereas the local density is significantly increased but still well below the saturation limit.

Simian Virus 40. Although we treated the density of (mobile) LecA on bacteria as an unknown but nonlimiting factor, the number of glycolipid receptors on the SV 40 virus capsids and its geometry are well known. To compare our results to the invagination of virus capsids, we assume for simplicity that the local concentration of Gb3 is as large as the receptor density, so the adhesion effect is maximal. We thus minimize $F_l + F_m$ with respect to h for a constant local density ρ to calculate the ratio of wrapping height h to capsid radius R:

$$\frac{h}{R} = \left(\rho\epsilon - \frac{2\kappa}{R^2}\right)\gamma^{-1} = \left(\frac{R^2}{\kappa}\rho\epsilon - 2\right)\frac{\kappa}{R^2}\,\gamma^{-1} =: (Z-2)\tilde{\gamma}^{-1}, \quad \textbf{[S14]}$$

where ε is the adhesion energy per glycolipid and ρ the local glycolipid concentration. The size R determines the strength of the influence of the bending rigidity κ on the wrapping of the capsid.

We calculate ρ by dividing the number of receptors [72 for the capsids (8)] by the surface $4\pi R^2$. The radii and adhesion energies (see ref. 8) for the receptor monomers, pentamers, and capsids as well as the derived quantities are given in Table S1.

All densities are far below the upper boundary for Gb3, $\rho_{max} = 1.25\ \mathrm{nm}^{-2}$. Because $Z < 2$ for the monomers and pentamers, Eq. **S14** has no positive solution for h, so without mechanisms other than described here no invagination would occur. The capsids will be just fully wrapped when $(Z-2)\tilde{\gamma}^{-1} = 2 \Leftrightarrow \tilde{\gamma}^{-1} \approx 2.3 \Leftrightarrow \gamma = 3 \cdot 10^{-5}\ \mathrm{J/m^2}$. Invaginations on GUVs induced by SV40 virus-like particles have been observed even with surface tensions in the order of $10^{-3}\ \mathrm{J/m^2}$ (see ref. 8), so other mechanisms have to be considered for the capsids as well.

1. Abe A, et al. (1992) Improved inhibitors of glucosylceramide synthase. *J Biochem* 111(2):191–196.
2. Winzer K, et al. (2000) The Pseudomonas aeruginosa lectins PA-IL and PA-IIL are controlled by quorum sensing and by RpoS. *J Bacteriol* 182(22):6401–6411.
3. Riedl J, et al. (2008) Lifeact: A versatile marker to visualize F-actin. *Nat Methods* 5(7): 605–607.
4. Helfrich W (1973) Elastic properties of lipid bilayers: Theory and possible experiments. *Z Naturforsch C* 28(11):693–703.
5. Deserno M, Bickel T (2003) Wrapping of a spherical colloid by a fluid membrane. *EPL* 62:767.
6. Reynwar BJ, et al. (2007) Aggregation and vesiculation of membrane proteins by curvature-mediated interactions. *Nature* 447(7143):461–464.
7. Deserno M (2004) Elastic deformation of a fluid membrane upon colloid binding. *Phys Rev E Stat Nonlin Soft Matter Phys* 69(3 Pt 1):031903.
8. Ewers H, et al. (2010) GM1 structure determines SV40-induced membrane invagination and infection. *Nat Cell Biol* 12(1):11–18, 1–12.
9. Blanchard B, et al. (2008) Structural basis of the preferential binding for globo-series glycosphingolipids displayed by Pseudomonas aeruginosa lectin I. *J Mol Biol* 383(4): 837–853.
10. Mahfoud R, Mylvaganam M, Lingwood CA, Fantini J (2002) A novel soluble analog of the HIV-1 fusion cofactor, globotriaosylceramide (Gb(3)), eliminates the cholesterol requirement for high affinity gp120/Gb(3) interaction. *J Lipid Res* 43(10):1670–1679.
11. Kucerka N, et al. (2008) Lipid bilayer structure determined by the simultaneous analysis of neutron and X-ray scattering data. *Biophys J* 95(5):2356–2367.

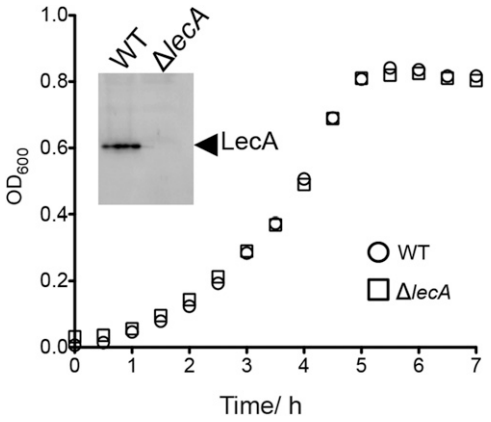

Fig. S1. Characteristics of *P. aeruginosa* PAO1 WT and Δ*lecA* mutant. Growth kinetics of *P. aeruginosa* PAO1 WT and Δ*lecA* cultures at 37 °C. PAO1 WT and Δ*lecA* exhibit the same growth kinetics. (*Inset*) Overnight cultures of *P. aeruginosa* PAO1 WT and Δ*lecA* were tested for LecA production by standard Western blot analysis, verifying the lack of LecA synthesis in the Δ*lecA* mutant.

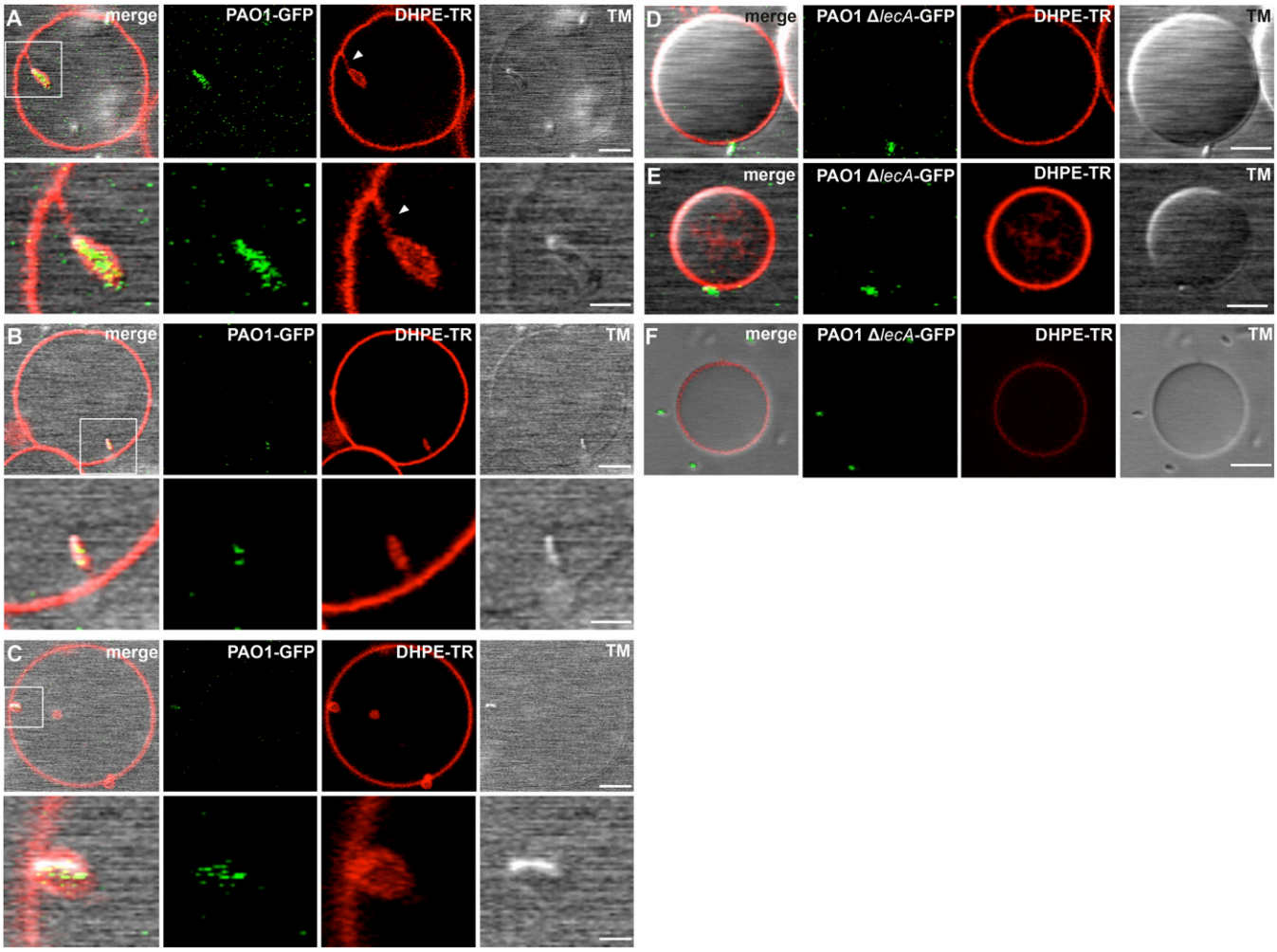

Fig. S2. Representative images of GUVs inoculated with *P. aeruginosa* PAO1 WT or Δ*lecA* mutant. (*A*–*C*) Images of GUVs as shown in Fig. 1 containing 5 mol% Gb3 inoculated with *P. aeruginosa* PAO1 WT or Δ*lecA*. (*D* and *E*) In *A* and *B*, a tether-like structure is visible between the membrane-wrapped bacterium and the outer GUV membrane (white arrowhead). Although PAO1 Δ*lecA* bacteria bound either horizontally or vertically to Gb3-containing GUVs, they do not induce membrane invaginations, as observed frequently for the WT strain. (*F*) In most cases PAO1 Δ*lecA* bacteria did not bind to Gb3-containing GUVs. (Scale bars, *A*–*C*, *Upper*, *D*, and *F*, 5 μm; *A*–*C*, *Lower*, and *E*, 2.5 μm.)

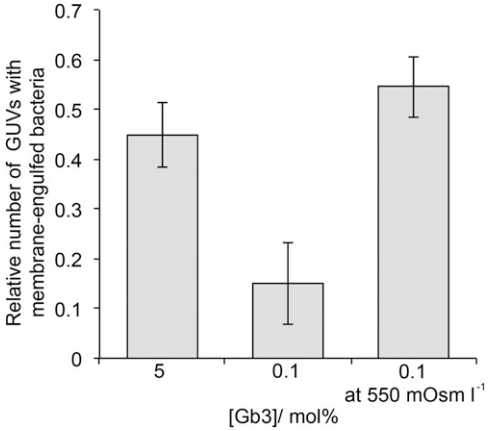

Fig. S3. Decrease in membrane tension facilitates the lipid zipper. Membrane tension of GUVs containing indicated Gb3 concentrations was decreased by exposure of GUVs to a hyperosmolar, external buffer solution (550 mOsm·L^{-1} outside buffer vs. 290 mOsm·L^{-1} inside buffer). Decrease of surface tension leads to an increase of GUVs showing membrane-wrapped bacteria. Relative numbers of GUVs containing membrane-wrapped *P. aeruginosa* PAO1 WT are shown. Numbers of invaginated GUVs were normalized to number of GUVs bound by bacteria. Bars represent mean values ± SEM of $n \geq 3$ independent experiments. In total ≥100 GUVs were analyzed (46 GUVs at 550 mOsm·L^{-1}).

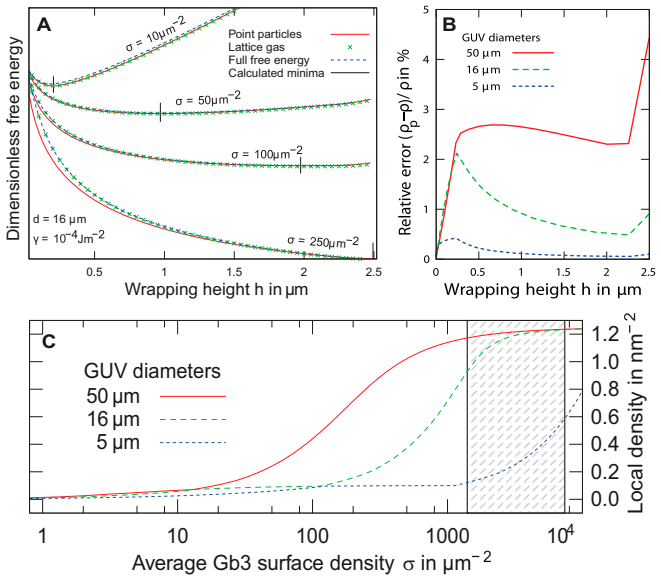

Fig. S4. (*A*) Numerically calculated full free energy (including the numerically evaluated free membrane part in Eq. **S2** and the free energy for the lattice gas in Eq. **S6**) for different surface densities σ. The perpendicular black lines show the minimum of the free energy. At these points the difference between the numerically calculated free energy and the used approximations are always minute, justifying the validity of the simplifications made. (*B*) Relative error of the local density ρ_P, for point particles (ignoring steric repulsion) in comparison with the saturating local densities ρ for the lattice gas. The relative error is always smaller than 5% in the relevant regime, which justifies the point-particle approximation. (*C*) Local Gb3 density as a function of the global density σ on the vesicle for different GUV diameters. Although the mobility of the Gb3 density leads to significantly enhanced local densities, the bacteria are always fully wrapped before the local density goes into saturation (compare with Fig. 2*C*).

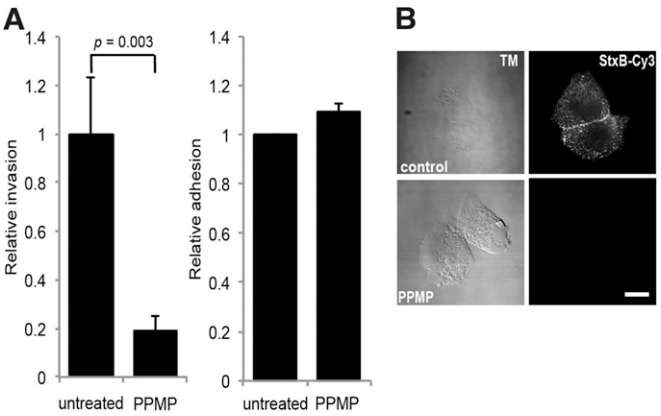

Fig. S5. Glycosphingolipid expression is a prerequisite for efficient *P. aeruginosa* uptake. (*A*, *Left*) Inhibition of glucosylceramide synthase by its substrate analog PPMP resulted in an 80% reduced invasiveness of *P. aeruginosa*. Internalization of *P. aeruginosa* PAO1 WT into untreated and PPMP-treated H1299 cells as measured by the invasion assay. (*A*, *Right*) Adhesion of *P. aeruginosa* PAO1 WT to untreated or PPMP-treated H1299 cells. All data represent mean values ± SEM for $n \geq 3$ experiments normalized to the WT. (*B*) Inhibition of glucosylceramide synthase by PPMP prevents binding of StxB-Cy3, which selectively binds to the glucosylceramide-derived GSL Gb3, to H1299 cells, representing the inhibition of GSL synthesis in H1299 cells by PPMP (*Lower*). TM, transmission. (Scale bar, 10 µm.)

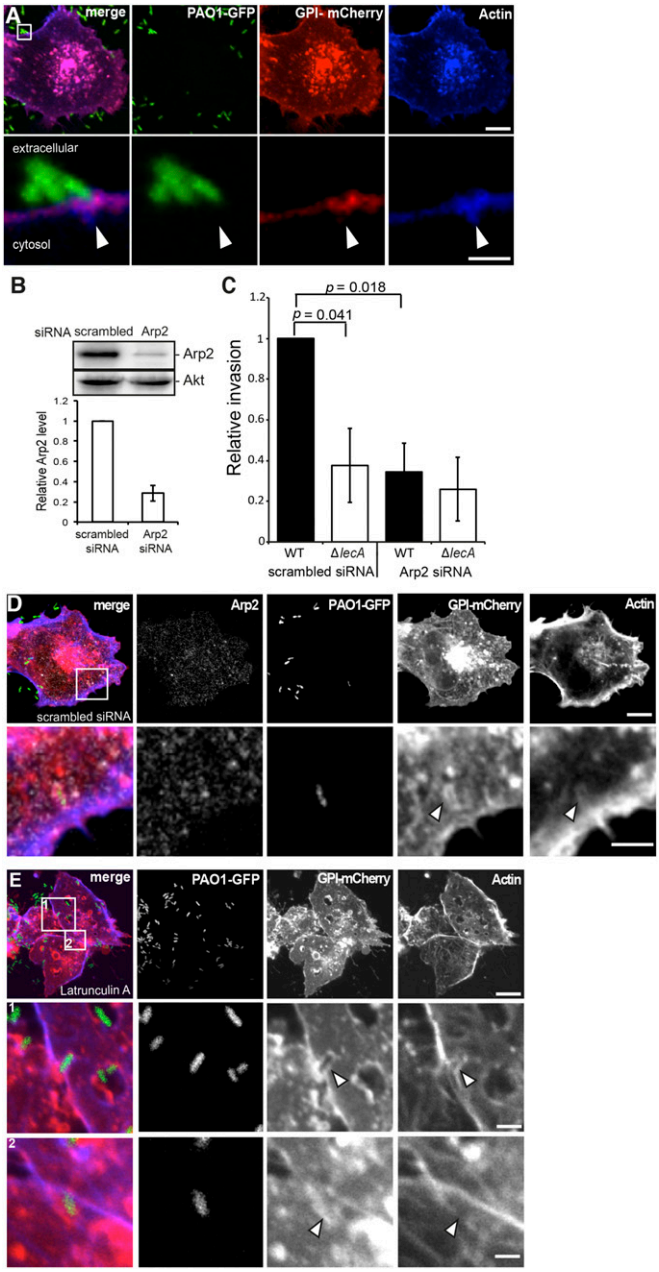

Fig. S6. *P. aeruginosa* induces negative PM curvature independently of actin polymerization. (*A*) GFP-tagged *P. aeruginosa* WT (PAO1-GFP) bound to an H1299 cell, which stably expresses GPI-mCherry as a PM marker. The lower panel represents a zoom of the squared area of the upper panel. Note that the PM is bent at the bacterial pole region at the cellular adhesion site, colocalizing with actin (arrowheads). Images were recorded from cells inoculated for 1 h with *P. aeruginosa* at MOI ~100. For better visualization of the curved PM, the contrast of the images in the lower panel was adjusted. (Scale bars, 10 μm and 2.5 μm, respectively.) (*B*) RNAi-mediated knockdown of Arp2 by siRNA was confirmed by Western blotting of uninfected H1299 cells. In total, Arp2 was reduced by 72% as quantified by densiometric analysis of Western blots compared with the level of Akt as a loading control ($n = 3$, mean ± SEM). (*C*) Invasion of Arp2-depleted H1299 cells by *P. aeruginosa* WT was significantly reduced by about 66%. The reduction of invasion for the *lecA* mutant (Δ*lecA*) by 75% was even more pronounced ($n = 4$ independent experiments, mean ± SEM, *P* value calculated by two-tailed, paired *t* test). These observations show that actin polymerization is in general crucial for a subset of *P. aeruginosa* cells to efficiently enter host cells. However, the initial steps of membrane invagination (Fig. 3*A*) do not require actin polymerization-dependent processes. (*D*) Control cells, corresponding to Arp2-depleted cells shown in Fig. 3*D*. Cells were transfected with scrambled siRNA and recorded with the same laser power and gains as the Arp2 siRNA-transfected cells. The same type of membrane invaginations (arrowhead) induced by *P. aeruginosa* WT as observed in untransfected (Fig. 3*A*) and Arp2-depleted H1299 cells (Fig. 3*D*) is visible. Images were recorded from cells inoculated with *P. aeruginosa* for 1 h at MOI ~100. (Scale bars, 10 μm and 2.5 μm, respectively.) (*E*) Complementary to the Arp2 knockdown approach we assessed the dependency of membrane invaginations on actin polymerization processes, which we inhibited by latrunculin A (0.1 μM). In latrunculin A-treated H1299 cells *P. aeruginosa* is localized in PM invaginations (arrowheads) at 1 h postinoculation (MOI ~100). The same type of localization can be seen in untreated cells (Fig. 3*A*) where bacteria are also engulfed by the host cell membrane. Actin-covered (zoom 1) as well as uncovered invaginations (zoom 2) were observed. Therefore, actin polymerization is not essential for membrane wrapping and invaginations. (Scale bars, 10 μm and 2.5 μm, respectively.)

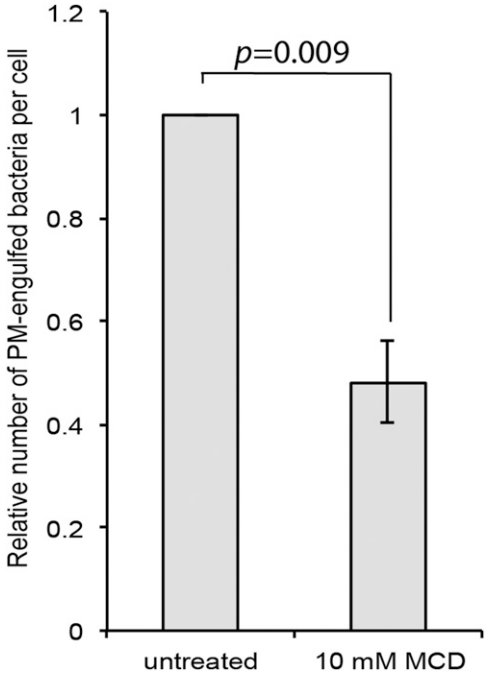

Fig. S7. Cholesterol depletion significantly reduces lipid zipper on H1299 cells. Cells expressing GPI-mCherry as a PM marker were cholesterol-depleted by treatment with 10 mM MCD for 30 min or left untreated. Afterward, cells were infected for 1 h at 37 °C with *P. aeruginosa* PAO1 WT. PM-engulfed bacteria per cell of untreated and MCD-treated cells were counted. Values represent mean values ± SEM of $n = 4$ independent experiments with >500 bacteria analyzed in total.

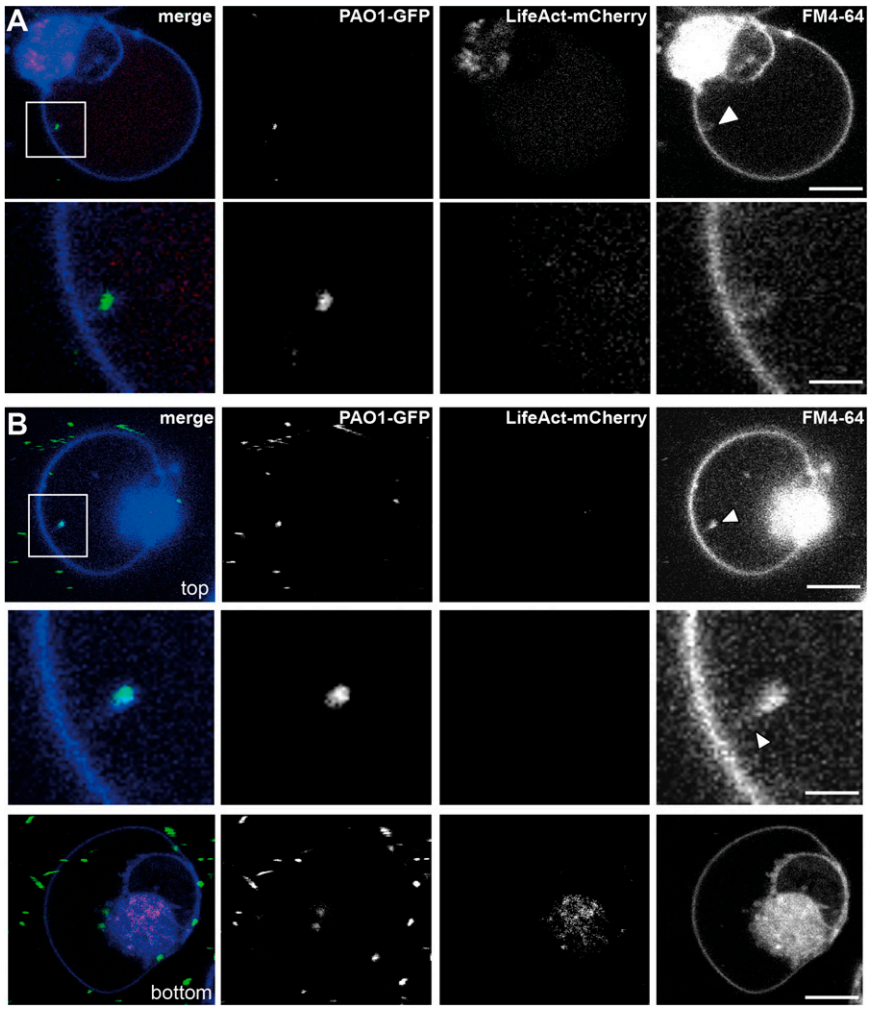

Fig. S8. *P. aeruginosa* induces membrane invaginations in PMS. (*A*) PMS were induced in H1299 cells stably expressing the actin polymerization marker LifeAct-mCherry. Actin was only visible in the cell body but was excluded in the PMS. PAO1 WT inoculated with PMS-containing cells induced a membrane invagination in the PMS, which was not covered by actin (arrowhead). Membrane was visualized by FM4-64 dye. (*B*) Example of another PMS induced from a H1299 cell, which shows a bacterial cell engulfed by the membrane of the PMS in the upper part of the cell body ("top"). Interestingly, the invaginated membrane is connected via a tether-like structure with the outer membrane of the PMS (arrowhead) as already observed in GUVs (Fig. S2*B*). The lower part ("bottom") shows actin in the remaining cell body. (Scale bars, 10 μm and 5 μm.)

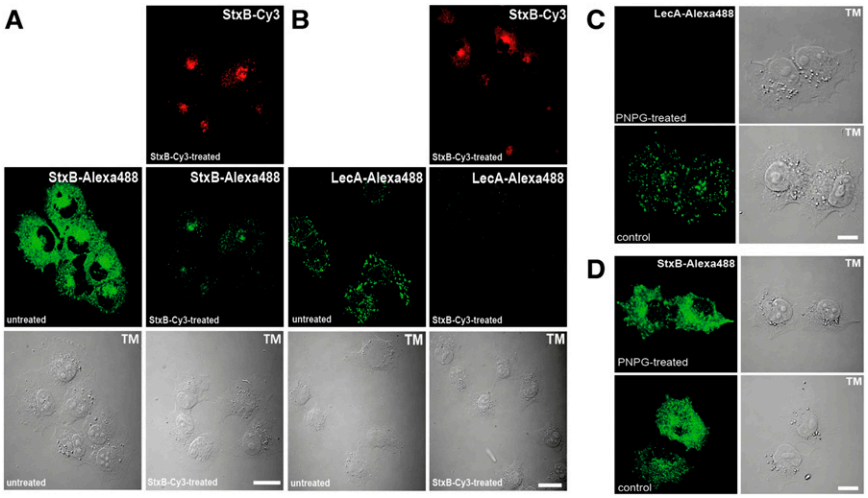

Fig. S9. Control of Gb3 depletion and LecA inhibition. (*A*) PM-localized Gb3 content of H1299 cells is significantly decreased by pretreatment with StxB-Cy3 as indicated by a strong reduction of StxB-Alexa488 uptake. (*B*) Decreased PM-localized Gb3 in H1299 cells results in significantly reduced LecA binding and uptake compared with untreated (control) cells. Furthermore, this indicates that Gb3 is a receptor for LecA. For comparison, untreated and StxB-Cy3–treated cells were imaged with equal laser power and gain settings for StxB-Alexa488 and LecA-Alexa488, respectively. (Scale bars, 20 μm.) (*C*) PNPG selectively inhibits LecA uptake. Binding and uptake of LecA-Alexa488 (*C*) and StxB-Alexa488 (*D*) after treatment of H1299 cells with PNPG was visualized. PNPG significantly impairs LecA but not StxB uptake. Images of Alexa488 fluorescence were recorded with equal laser power and gain settings. TM, transmission. (Scale bars, 10 μm.)

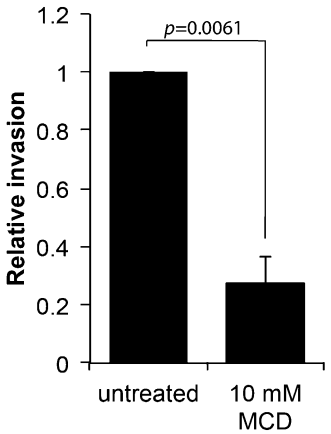

Fig. S10. Cholesterol depletion significantly reduces host cell invasion by *P. aeruginosa*. Invasion of PAO1 WT into cholesterol-depleted H1299 cells was quantified. Values represent mean values ± SEM of $n = 4$ independent experiments.

Table S1. Comparison to SV40 capsid proteins

Parameter	Monomer	Pentamer	Capsid	Large spheres
r, nm	5	12	50	250
ε	2 k_BT	10 k_BT	10 k_BT	10 k_BT
ρ	1.6×10^{-3} nm^{-2}	5.5×10^{-4} nm^{-2}	2.3×10^{-3} nm^{-2}	2.3×10^{-3} nm^{-2}
Z	$Z = 0.008$	$Z = 0.04$	$Z - 2 = 0.86$	$Z - 2 = 70$
$\tilde{\gamma}$			0.03–32	0.001–1.3